



Study on the Productivity of Fractured Horizontal Wells in Shale Gas Reservoirs Considering Staggered Fracture Model

Xin Huang¹(✉), Rui-han Zhang¹, Lie-hui Zhang¹, Yu-long Zhao¹, and Shan Yuan²

¹ The State Key Laboratory of Oil and Gas Reservoir Geology and Exploitation, Southwest Petroleum University, Chengdu, China

huangxin203@163.com

² Research Institute of Exploration and Development, PetroChina Southwest Oil & Gas Field Company, Chengdu, China

Abstract. The well plant operation mode with high integration degree is widely adopted for shale gas reservoir development. In order to study the production dynamics of fractured horizontal wells in staggered placement mode, multiple seepage mechanisms of shale gas at the microscopic scale are considered, and a reservoir-fracture-wellbore coupled point source function flow model is developed based on the pressure drop superposition principle to investigate the factors influencing the production capacity of fractured horizontal wells in staggered placement mode. The study shows that not considering the microscopic seepage mechanism will overestimate the production of shale gas fractured horizontal wells, in which viscous flow makes the largest contribution to gas flow; the larger the overlap area of adjacent gas well modifications, the smaller the gas well production, and the decreasing production increases with the increase of the overlap area, so shale gas production platforms should avoid the overlap of modifications between adjacent wells; with the increase of well spacing, the gas well production increases, but the increase gradually decreases. The optimal well spacing exists between platform production wells. The study considers the microscopic seepage mechanism of shale gas and combines the fractured horizontal well capacity model to realize the study of the capacity dynamics of staggered fractured horizontal wells, which provides a reference for the study of multi-well production capacity.

Keywords: Staggered fracture · Fractured horizontal well · Shale gas · Apparent permeability · Productivity research

1 Introduction

Shale gas, as a kind of clean, medium and low carbon energy, is the main target of realizing China's carbon neutral goal in the traditional fossil energy field [1]. In the context of cost reduction and efficiency improvement of shale gas development investment benefits, the shale gas well plant operation mode has become the main technical means

to develop shale gas reservoirs nowadays because of its unique advantages in terms of footprint, integrated drilling and completion technology, trip fracturing and increased control area of a single well [2–5]. A hybrid well network with multiple combinations of straight, directional and horizontal well types can maximize the use of isolated resource bodies, which is most widely used in clustered horizontal well sets [6]. The well-to-well and fracture-to-fracture layout affects the horizontal well fracturing method and post-fracture production dynamics. The staggered fracture model can avoid the inter well interference caused by pressure channeling between horizontal wells and make full use of inter-fracture stress interference to enhance the complexity of hydraulically fractured fractures, thus enhancing the transformation effect.

Shale gas is mainly stored in the matrix nanopores in both free and adsorbed states, and currently, two main types of molecular simulation and continuous flow models are used by researchers to study it. Molecular simulation is mainly based on molecular dynamics [7] and lattice Boltzmann method [8], which can realize the intuitive simulation of single or multiple gas molecules, but the combination with macroscopic flow still needs to be studied; continuous flow models are mostly based on capillary bundle model to establish gas apparent permeability equations, and characterize the permeability mechanisms such as viscous flow, molecular diffusion and surface adsorption diffusion of shale gas, and in the construction of apparent permeability equations There are mainly two ways of linear superposition [9–11] and weighted superposition [12–15], but few studies have been reported on the apparent permeability of pore gas flow characteristics that distinguish between organic and inorganic pores. Shale pneumatic fracture horizontal well capacity prediction models mainly include two types of semi-analytical models and numerical models [16], semi-analytical models [17, 18] by dividing the fracture micro-element body, establishing matrix and fracture system coefficient solution matrix, and solving the sparse matrix for production dynamic prediction; numerical models [19–21] based on the idea of grid discretization, numerical discretization of the spatial and temporal terms of the percolation equation, solving the partial differential equations to predict the production dynamics. At present, there are few horizontal well capacity models considering staggered seam conditions. Therefore, it is of practical importance to study the capacity model of fractured horizontal wells in staggered spacing mode to predict the production dynamics.

In this paper, we comprehensively consider the multiple transport mechanisms of shale gas at the micro and nano scales, distinguish the gas flow channels into two categories: organic and inorganic pores, and establish the apparent permeability model of gas flow. On this basis, a mathematical model of reservoir-fracture-wellbore coupled point source function is established by the pressure drop superposition principle, and the numerical solution of the model is obtained by solving and calculating the sparse matrix using the numerical iteration method. The effects of micro-scale flow mechanism, well spacing, and modified overlap zone on the capacity of horizontal wells are analyzed.

2 Mathematical Model

2.1 Gas Multiple Flow Mechanism

The flow of shale gas in the pores of shale matrix can be classified into three categories: viscous flow, molecular diffusion and surface adsorption diffusion. In this paper, the fractal capillary bundle model is used to model the gas flow in shale micro and nano scale pores (as shown in Fig. 1). Based on the reference [22], the molar mass flux in a single capillary of organic matter under the consideration of real gas effects is calculated as

$$\begin{aligned}
 J(\lambda) = J_v + J_t + J_s = & \frac{\pi\lambda^4\rho_g}{128\mu_g M} \frac{\Delta p}{L_t} + \frac{\pi\lambda^3}{12} \frac{K_n}{K_n + 1} \sqrt{\frac{8Z}{\pi MRT}} \frac{p}{Z} c_g \frac{\Delta p}{L_t} \\
 & + \pi(\lambda d_m \theta - d_m^2 \theta^2) D_s C_L \left[\frac{Z p_L - p p_L \frac{\partial Z}{\partial p}}{(Z p_L + p)^2} \right] \frac{\Delta p}{L_t} \quad (1)
 \end{aligned}$$

where: J_v, J_t, J_s represent the molar mass fluxes of viscous flow, molecular diffusion and surface adsorption diffusion motion, mol/s; ρ_g denotes gas density, kg/m³; μ_g denotes gas viscosity, mPa·s; M denotes gas molar mass, kg/mol; d_m denotes methane molecular diameter, m; p denotes pore pressure, MPa; T denotes formation temperature, K. B_g denotes the gas volume coefficient, uncaused; θ denotes the coverage of the adsorption layer on the pore surface, dimensionless; D_s denotes the gas surface diffusion coefficient, m²/s; p_L denotes the gas Langmuir adsorption pressure, MPa; L_t denotes the true capillary length, m.

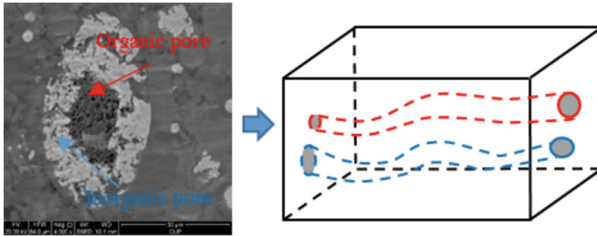


Fig. 1. Fractal capillary bundle model based on organic and inorganic pores

Based on the fractal theory, the total mass flux $J(\lambda)$ in a single capillary is integrated over the minimum and maximum capillary diameters to obtain the total molar mass of the rock matrix tortuous capillary bundle with the total number of capillaries N_F .

$$Q_T = - \int_{\lambda_{\min}}^{\lambda_{\max}} J(\lambda) dN \quad (2)$$

By associating Eq. (2) with the Darcy percolation molar mass equation, the apparent gas permeability in the shale organic matter micro and nano pores considering viscous flow, molecular diffusion and surface diffusion in the real state can be obtained as follows.

$$k_{Om} = \frac{\pi \lambda_{Omax}^{3+D_T}}{128 L_0^{D_T+1}} \frac{D_f}{3 - D_f + D_T} + \frac{10^{-9} \times \pi \mu_g}{12} \sqrt{\frac{8ZRT}{\pi M}} \frac{D_f \lambda_{Omax}^{D_f}}{L_0^{D_T+1}} c_g \int_{\lambda_{Omin}}^{\lambda_{Omax}} \frac{K_n}{K_n + 1} \lambda^{1-D_f+D_T} d\lambda$$

$$+ 10^{-9} \times \pi D_s C_L \left[\frac{Z_{PL} - PPL \frac{\partial Z}{\partial p}}{(Z_{PL} + p)^2} \right] \frac{D_f d_m \theta \mu_g M}{\rho_g L_0^{D_T+1}} \left[\begin{array}{l} \frac{\lambda_{Omax}^{D_T}}{D_T - D_f} \left(1 - \left(\frac{\lambda_{Omin}}{\lambda_{Omax}} \right)^{D_T - D_f} \right) \\ - \frac{d_m \theta \lambda_{Omax}^{D_T-1}}{D_T - D_f - 1} \left(1 - \left(\frac{\lambda_{Omin}}{\lambda_{Omax}} \right)^{D_T - D_f - 1} \right) \end{array} \right] \quad (3)$$

where: λ_{Omax} denotes the maximum diameter of organic matter pore, m; λ_{Omin} denotes the minimum diameter of organic matter pore, m; C_L denotes the maximum adsorption capacity of shale rock sample; D_f denotes the fractal dimension, dimensionless; D_T denotes the meandering fractal dimension, dimensionless; L_0 denotes the straight edge length of rock sample, m.

Similarly, neglecting surface adsorption diffusion in inorganic pores yields the inorganic pore fractal apparent permeability.

$$k_{Im} = \frac{\pi \lambda_{Imax}^{3+D_T}}{128 L_0^{D_T+1}} \frac{D_f}{3 - D_f + D_T} + \frac{10^{-9} \times \pi \mu_g}{12} \sqrt{\frac{8ZRT}{\mu M}} \frac{D_f \lambda_{Imax}^{D_f}}{L_0^{D_T+1}} c_g \int_{\lambda_{Imin}}^{\lambda_{Imax}} \frac{K_n}{K_n + 1} \lambda^{1-D_f+D_T} d\lambda \quad (4)$$

where: λ_{Imax} indicates the maximum diameter of inorganic pore, m; λ_{Imin} indicates the minimum diameter of inorganic pore, m.

The equation for calculating the apparent permeability of shale gas reservoir micro and nano scale seepage can be expressed as

$$k_{app} = \varepsilon k_{Om} + (1 - \varepsilon) k_{Im} \quad (5)$$

where: ε indicates the organic matter percentage, dimensionless.

2.2 Mathematical Model of Seepage

For staggered fractured shale gas reservoir fracturing platform well sets, the horizontal wells are numbered 1 to N . Taking three horizontal wells as an example, the intermediate horizontal wells are numbered 1 to N from the heel end to the toe end of the fracture in order, and the horizontal wells on the outer flanks are numbered 1 to $N + 1$ (as shown in Fig. 2). By discretizing each hydraulic fracture into $2n$ parts and dividing each flank into n parts, with the upper flank represented by 1 and the lower flank represented by 2, all hydraulic fractures in a fractured well group are discretized into a total of $2n(3N + 2)$ fracture grid cells (as shown in Fig. 3(b)).

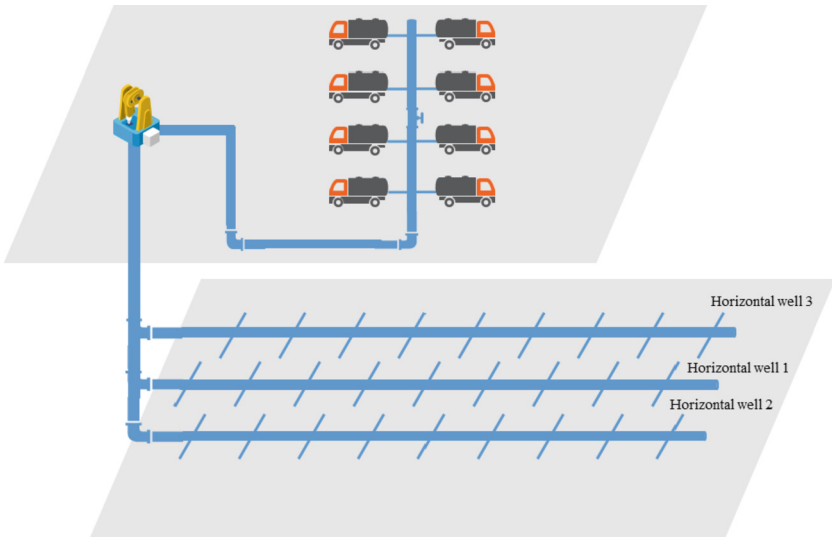


Fig. 2. Schematic diagram of shale gas fracturing well production platform

The model is assumed as follows: ① gas reservoir is a box-shaped closed gas reservoir; ② vertical fracture penetrates the reservoir; ③ horizontal well is considered to be infinite inflow; ④ gas reservoir is considered to be single-phase gas flow and the effect of gravity is not considered; ⑤ fluid flows into the horizontal wellbore through the fracture.

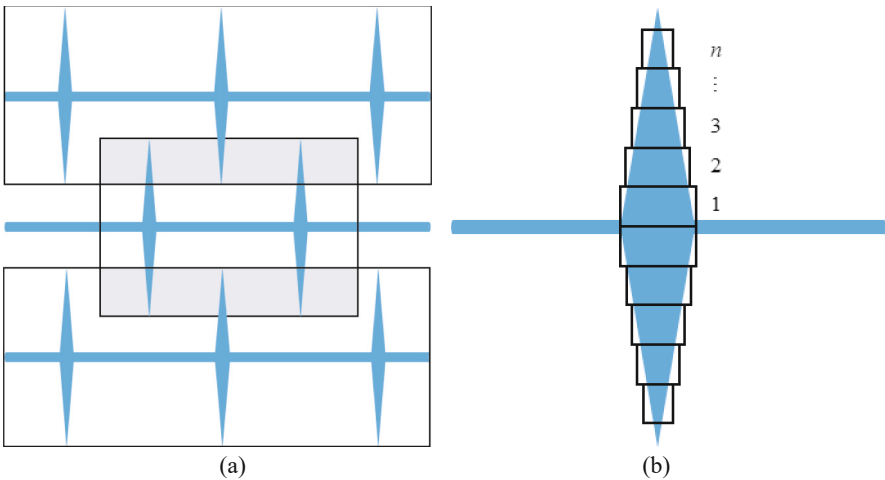


Fig. 3. a. Overlap of fracture modification zones of adjacent production wells (grey part is the overlap zone); b. Grid dissection of single fracture.

For closed-boundary fractured horizontal wells with no fluid flow on the boundary at the initial production stage, the source function is used to solve the gas percolation

equation and according to the Newman integral, the pressure drop generated by the fluid flowing at a point (x_i, y_i, z_i) along the fracture wall to any point (x, y, z) in the gas reservoir is

$$p_{\text{int}}^2 - p^2(x, y, z, t) = \frac{2q(x_i, y_i, z_i, t)\mu_g p_{\text{sc}} ZT}{\phi C_t abh T_{\text{sc}}} \int_0^t S(x, t) \cdot S(y, t) \cdot S(z, t) dt \quad (6)$$

where

$$S(x, t) = 1 + 2 \sum_{n=1}^{\infty} \exp\left(-\frac{k_{\text{app}}}{\mu_g C_t \phi} \frac{n^2 \pi^2 t}{a^2}\right) \cos \frac{n\pi x_w}{a} \cos \frac{n\pi x}{a}$$

$$S(y, t) = 1 + 2 \sum_{m=1}^{\infty} \exp\left(-\frac{k_{\text{app}}}{\mu_g C_t \phi} \frac{m^2 \pi^2 t}{b^2}\right) \cos \frac{m\pi y_w}{b} \cos \frac{m\pi y}{b}$$

$$S(z, t) = 1 + 2 \sum_{l=1}^{\infty} \exp\left(-\frac{k_{\text{app}}}{\mu_g C_t \phi} \frac{l^2 \pi^2 t}{h^2}\right) \cos \frac{l\pi z_w}{h} \cos \frac{l\pi z}{h}$$

where: p_{int} denotes the original formation pressure, MPa; C_t denotes the reservoir rock compression coefficient, MPa^{-1} ; a denotes the calculated model reservoir length, m; b denotes the calculated model reservoir width, m; h denotes the calculated model reservoir thickness, m; p_{sc} denotes the standard condition pressure, MPa; T_{sc} denotes the standard condition temperature, K; n, m, l denote the discrete grid cell scale in $x, y,$ and z directions.

Equation (6) represents the pressure drop generated by each grid cell, for all fracture grids by the principle of pressure drop superposition, the total pressure drop generated at any point (x, y, z) in the gas reservoir at time t is

$$p_{\text{int}}^2 - p^2(x, y, z, t) = \sum_{m=1}^{N+1} \sum_{l=1}^{N+1} \sum_{k=1}^N \sum_{j=1}^2 \sum_{i=1}^n q(m, l, k, j, i, t) R(x, y, z, t) \quad (7)$$

where $R(x, y, z, t)$ is defined as the gas reservoir pressure drop coefficient.

$$R(x, y, z, t) = \frac{2\mu_g p_{\text{sc}} ZT}{\phi C_t abh T_{\text{sc}}} \int_0^t S(x, t) \cdot S(y, t) \cdot S(z, t) dt \quad (8)$$

Using different grid values for different grid cells and considering the one-dimensional linear flow in the hydraulically fractured fracture, the pressure drop from any point i in the fracture to the wellbore can be obtained from Darcy's law as

$$p_i^2(t) - p_{\text{wf}}^2 = \frac{2\mu_g p_{\text{sc}} ZT}{k_f h T_{\text{sc}}} \left\{ \sum_{k=1}^{i-1} \left(q_k \sum_{j=1}^k \frac{\Delta l_{j+1, j}}{w_j} \right) + \sum_{m=i}^n \left[q_m \left(\sum_{j=1}^{i-1} \frac{\Delta l_{j+1, j}}{w_j} + \frac{\Delta l_{i+1, i}}{2w_i} \right) \right] \right\} \quad (9)$$

where: k_f denotes hydraulic fracture permeability, mD; p_{wf} denotes bottom hole flow pressure, MPa; $\Delta l_{i, i-1}$ denotes the distance between node i and node $i-1$, m; w_i denotes the average width of fracture micro-element i , m.

For a hydraulic fracture grid cell, assuming that the fracture is filled with fluid, the flow into the fracture grid cell is equal to the flow out according to the law of conservation of mass, which

$$q_{in}(m, l, k, j, i, t) = q_{out}(m, l, k, j, i, t) \tag{10}$$

Without considering the wellbore storage phenomenon, the coupled gas reservoir-fracture-wellbore flow and seepage equation is established by associating Eq. (7) and Eq. (9) as

$$p_{int}^2 - p_{wf}^2 = \sum_{m=1}^{N+1} \sum_{l=1}^{N+1} \sum_{k=1}^N \sum_{j=1}^2 \sum_{i=1}^n q(m, l, k, j, i, t) R(x, y, z, t) + \frac{2\mu p_{sc} Z T}{k_f h T_{sc}} \left\{ \sum_{k=1}^{i-1} \left(q_k \sum_{j=1}^k \frac{\Delta l_{j+1,j}}{w_j} \right) + \sum_{m=i}^n \left[q_m \left(\sum_{j=1}^{i-1} \frac{\Delta l_{j+1,j}}{w_j} + \frac{\Delta l_{i+1,i}}{2w_i} \right) \right] \right\} \tag{11}$$

3 Model Solving

The total pressure drop generated by $2n(3N + 2)$ fracture grid cells at moment t for any one grid cell can be obtained for Eq. (11), which in turn is transformed into a system of $2n(3N + 2)$ linear equations with the gas reservoir pressure drop coefficient of

$$M = \begin{bmatrix} R(1, 1) & R(1, 2) & \dots & R(1, 2n \times (3N + 2)) \\ R(2, 1) & R(2, 2) & \dots & R(2, 2n \times (3N + 2)) \\ \vdots & \vdots & & \vdots \\ R(2n \times (3N + 2), 1) & R(2n \times (3N + 2), 2) & \dots & R(2n \times (3N + 2), 2n \times (3N + 2)) \end{bmatrix} \tag{12}$$

For any hydraulic fracture with $2n$ parts discretization, the matrix of pressure drop coefficient in fracture is obtained as

$$AI = \begin{bmatrix} 0.5F_1 & 0.5F_1 & 0.5F_1 & \dots & 0.5F_1 \\ 0 & 0.5F_2 + F_1 & 0.5F_2 + F_1 & \dots & 0.5F_2 + F_1 \\ 0 & 0 & 0.5F_3 + F_2 + F_1 & \dots & 0.5F_3 + F_2 + F_1 \\ \vdots & \vdots & \vdots & & \vdots \\ 0 & 0 & 0 & \dots & 0.5F_n + \sum_{i=1}^{n-1} F_i \end{bmatrix} \tag{13}$$

where

$$F_i = \frac{2\mu p_{sc} Z T}{k_f h T_{sc}} \frac{\Delta l_{i+1,i}}{w_i} \tag{14}$$

Combining the single-wing crack in-seam pressure drop coefficient matrix blocks to obtain a diagonal square matrix of order $6N + 4$, the coefficient matrix of the crack in-seam pressure drop equation is

$$F = \begin{bmatrix} AI & Z & Z \\ Z & \ddots & Z \\ Z & Z & AI \end{bmatrix} \tag{15}$$

Rewriting Eq. (11) into matrix form.

$$Aq = p \tag{16}$$

where

$$A = M + F$$

$$q = [q_1 \ q_2 \ q_3 \ \dots \ q_{2n \times (3N+2)}]^T$$

$$p = [p_{int}^2 - p_{wf}^2 \ p_{int}^2 - p_{wf}^2 \ p_{int}^2 - p_{wf}^2 \ \dots \ p_{int}^2 - p_{wf}^2 \ p_{int}^2 - p_{wf}^2]^T$$

The Gauss-Seidel iterative method is applied to Eq. (16) for the computational solution of the system of sparse matrix equations.

4 Example Application and Analysis

For three fractured horizontal wells in a fractured well production platform in a shale gas reservoir in the Fuling area of China, a capacity calculation analysis was carried out, and one of the horizontal well parameters was selected as the base input parameter, and the other two wells were calculated using this well data (see Table 1).

Table 1. Basic parameters of the model.

Parameter	Value	Parameter	Value
a , m	1600	p_L , MPa	4.48
b , m	600	V_L , m ³ /kg	2.72×10^{-3}
h , m	50	t , d	1560
D_T , -	1.1	D_f , -	1.2
p_{int} , MPa	25	μ_g , mPa·s	0.02
C_t , MPa ⁻¹	2.3×10^{-2}	p_{wf} , MPa	15
T , K	363	N_F , -	14
ϵ , -	0.05	ϕ , -	0.03

(continued)

Table 1. (continued)

Parameter	Value	Parameter	Value
x_f , m	180	ρ_g , kg/m ³	400
λ_{Omax} , nm	60	λ_{Imax} , nm	400
λ_{Omin} , nm	3	λ_{Imin} , nm	20

The model was validated by comparing the actual production data of the mine using the capacity model established in this paper (as shown in Fig. 4). After 1560d of production, the model predicted a daily gas production of 2.06×10^4 m³/d, and the actual daily gas production was 2.33×10^4 m³/d, with a calculation error of 11.6%. The model calculates the cumulative gas production as 0.8×10^8 m³, and the actual cumulative gas production is 0.7×10^8 m³, with a calculation error of 14.3%. The calculation error meets the requirements of the mine.

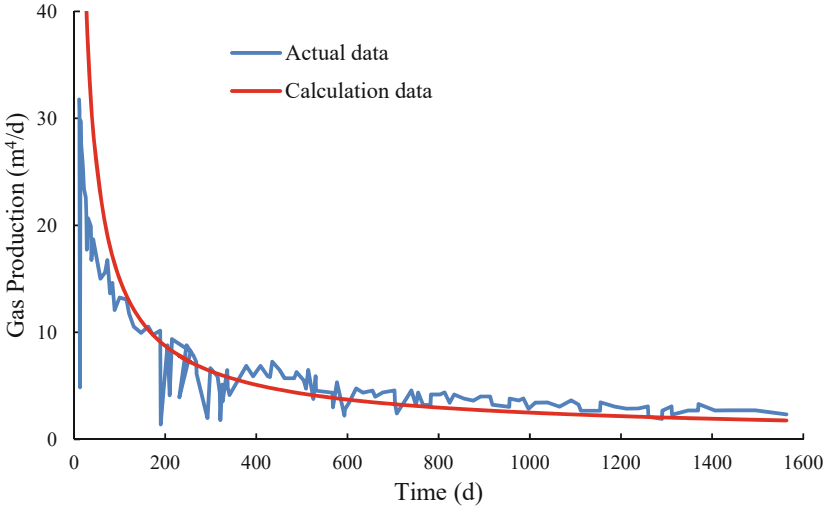


Fig. 4. Comparison of model calculated production and actual production

4.1 Micro-scale Flow Mechanism

Multiple flow mechanisms are the main feature that distinguishes shale gas flow in reservoir porous media from conventional gas reservoirs. Figure 5 shows the effect of micro flow mechanisms on the production of shale gas fractured horizontal wells. The cumulative gas production is 1.28×10^8 m³ after 1560d without considering the micro flow mechanism, and 1.02×10^8 m³ after 1560 d with considering the micro flow mechanism, with a 20% difference in production between the two. Not considering the microscopic flow mechanism of gas will underestimate the gas production capacity of gas wells, and this error will be further magnified in the stable production stage of

gas wells. The gas adsorbed in the shale matrix will desorb into the fractures during the steady production stage, increasing the gas supply replenishment. This shows the influence of shale gas micro flow mechanism on production, therefore, a comprehensive gas apparent permeability model considering all aspects needs to be constructed when doing capacity evaluation of fractured horizontal wells in shale gas reservoirs.

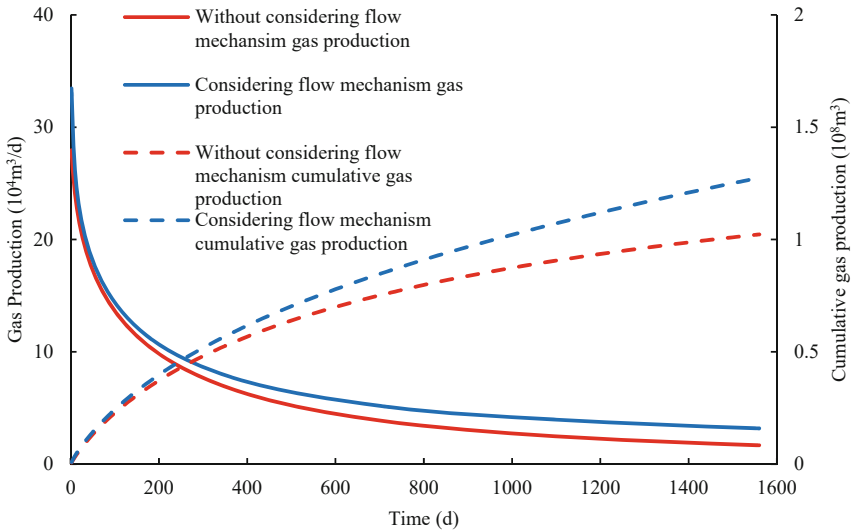


Fig. 5. Effect of microscopic seepage mechanism on shale gas well production

4.2 Well Spacing

Shale gas well plant platforms should be designed with reasonable well spacing to ensure maximum control of reserves and to avoid inter-well construction interference and production interference as much as possible. Figure 6 represents the effect of well spacing on the production of shale gas horizontal wells. As can be seen from the figure, with the increase of well spacing daily gas production and cumulative gas production are gradually increasing, and when the well spacing increases from 220 m to 260 m and 300 m, the cumulative gas production increases by 38% and 55% respectively after 1560 d of production, and the increase is slowing down. At the mine site, the number of wells drilled in the production platform will decrease without increasing the well field area, and the area of regional control reserves will decrease. Decreasing the well spacing increases the probability of pressure fracture between adjacent wells, and the optimal length of adjacent well spacing exists at the design site with the return on investment ratio as the goal.

4.3 Modification of Overlapping Areas

Although fracture scattering between adjacent wells was avoided in the staggered fracture placement mode, the phenomenon of overlapping transformation areas still existed (see

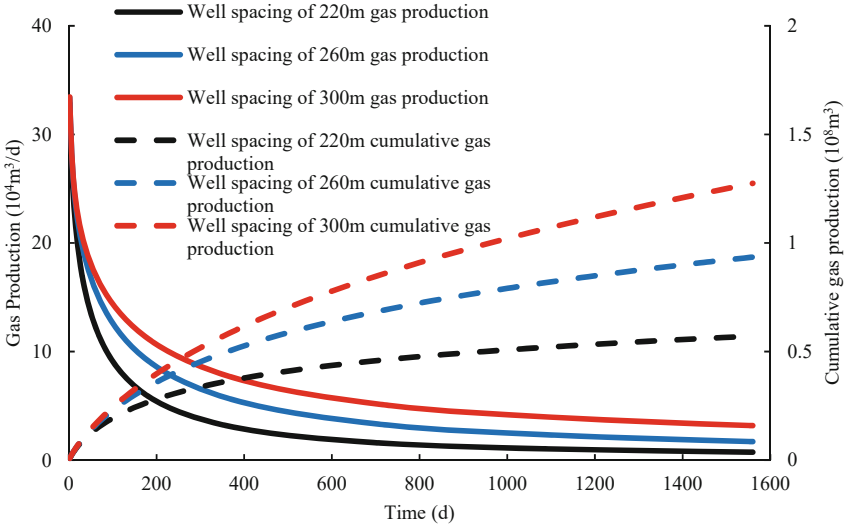


Fig. 6. Effect of well spacing on shale gas well production

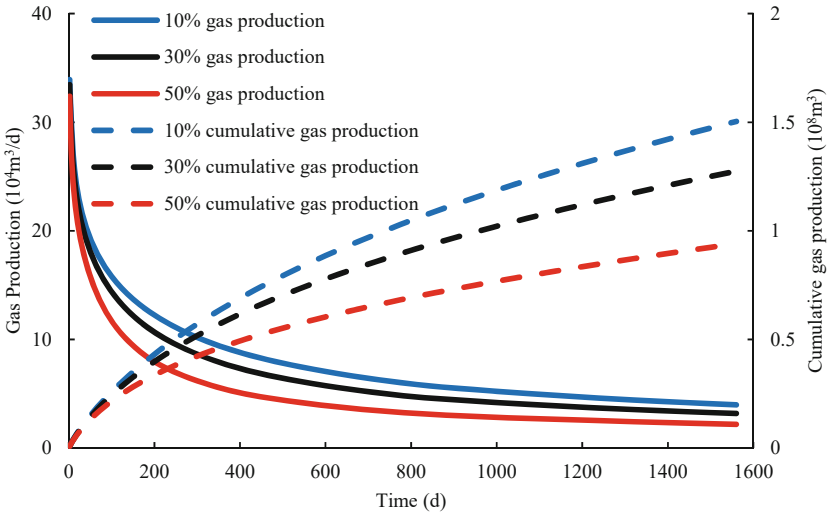


Fig. 7. Impact of modified overlap zones on shale gas well production

Fig. 7). At a fixed well spacing of 300m, the corresponding cumulative gas production volume decreases from 150 million to 120 million and 0.9 billion cubic meters when the proportion of the reformation overlap area is increased from 10% to 30% and 50% by increasing the hydraulic fracture length. This is due to the fact that the larger the proportion of the transformation volume overlap, the smaller the effective transformation volume of shale gas wells and the reduced degree of shale reservoir utilization. Therefore,

effectively reducing the modification volume overlap ratio can improve the production of horizontal shale gas wells in staggered seam mode, and the optimal modification volume overlap ratio exists.

5 Conclusion

This study considers the microscopic seepage mechanism of shale gas and combines the fractured horizontal well capacity model to realize the study of the capacity dynamics of staggered fractured horizontal wells. The main conclusions of this paper are as follows:

- (1) The production dynamics of shale gas-pressure fractured horizontal wells produced by the well plant model is influenced by the adjacent gas wells, and the fracture arrangement pattern and fracture morphology affect the production dynamics of gas wells. The reservoir-fracture-wellbore coupled seepage model established using the pressure drop superposition principle can be used to predict the production of horizontal wells in the staggered fracture arrangement mode.
- (2) Micro-flow mechanism has an important impact on shale gas well production. The cumulative gas production considering the micro-percolation mechanism is 1.2 times higher than that without considering the micro-percolation mechanism; the smaller the well spacing between horizontal wells, the smaller the production, but the decreasing relationship between the two is not linear. The production rate increases gradually with increasing well spacing, and there is an economic optimal well spacing.
- (3) The problem of overlap of the transformation area will inevitably occur in the well plant cluster platform production wells, and the overlap of the transformation area will lead to the reduction of gas well production, and the larger the overlap ratio, the smaller the production. However, the magnitude of production reduction gradually decreases, and there is an optimal transformation volume overlap ratio. When fracturing, it is necessary to see the disadvantages of production reduction caused by the overlapping of the modification volume, but also to recognize the advantages of controlling more isolated resource bodies between wells, and choose an optimal modification volume overlap ratio.

Acknowledgments. This work was supported by the China Postdoctoral Science Foundation (No.2020M673287), Science and Technology Cooperation Project of the CNPC-SWPU Innovation Alliance (Grant No. 2020CX030202).

References

1. Zou, C., Xiong, B., Xue, H., et al.: The role of new energy in carbon neutral. *Petrol. Explor. Develop.* **48**(2), 1–10 (2021)
2. Zhang, J., Tao, J., Li, Z., et al.: Prospect of deep shale gas resources in China. *Nat. Gas. Ind.* **41**(1), 15–28 (2021)

3. Zou, C., Zhao, Q., Cong, L., et al.: Development progress, potential and prospect of shale gas in China. *Nat. Gas. Ind.* **41**(1), 1–14 (2021)
4. Jiao, F.: Re-recognition of “unconventional” in unconventional oil and gas. *Petrol. Explor. Develop.* **46**(5), 803–810 (2019)
5. Guo, X., Hu, D., Wei, Z., et al.: Discovery and exploration of Fuling shale gas field. *China Petrol. Explor.* **21**(3), 24–37 (2016)
6. Zhang, J., Fan, Q., Wang, Y., et al.: mixed large well pattern development technology of tight sandstone gas in Sulige Gas Field Ordos Basin. *Xinjiang Petrol. Geol.* **40**(6), 714–719 (2019)
7. Vandembroucke, M.: Kerogen: from types to models of chemical structure. *Oil Gas Sci. Technol.* **58**(2), 243–269 (2003)
8. Luan, H.B., Xu, H., Chen, L., et al.: Evaluation of the coupling scheme of FVM and LBM for fluid flows around complex geometries. *Int. J. Heat Mass Transf.* **54**(9), 1975–1985 (2011)
9. Su, Y., Sheng, G., Wang, W., et al.: A multi-media coupling flow model for shale gas reservoirs. *Nat. Gas Indust.* **36**(2), 52–59 (2016)
10. Zhang, L., Shan, B., Zhao, Y., et al. Establishment of apparent permeability model and seepage flow model for shale reservoir. *Lithol. Reserv.* **29**(6), 108–118 (2017)
11. Civan, F., Rai, C.S., Sondergeld, C.H.: Shale-gas permeability and diffusivity inferred by improved formulation of relevant retention and transport mechanisms. *Transp. Porous Media* **86**(3), 925–944 (2011)
12. Wu, K., Chen, Z., Li, X., et al.: Real gas transport through nanopores of varying cross-section type and shape in shale gas reservoirs. *Chem. Eng. J.* **281**(6), 813–825 (2015)
13. Ren, L., Shu, L., Hu, Y., et al.: Analysis of gas flow behavior in nano-scale shale gas reservoir. *J. Southwest Petrol. Univ. (Sci. Technol. Ed.)* **36**(5), 112–115 (2014)
14. Ren, W., Li, G., Tian, S., et al.: An analytical model for real gas flow in shale nanopores with non-circular cross-section. *AIChE J.* **62**(8), 2893–2901 (2016)
15. Wu, K., Li, X., Chen, Z.: A model for gas transport through nanopores of shale gas reservoirs. *Acta Petrolei Sinica* **36**(7), 837–848 (2015)
16. Li, Y., Liu, X., Hu, Z., et al.: Summary of numerical models for predicting productivity of shale gas horizontal wells. *Adv. Earth Sci.* **35**(4), 350–362 (2020)
17. Hu, Y., Pu, X., Zhao, J., et al.: Production simulation of staged multi-cluster fractured horizontal wells with complex hydraulic fracture in shale gas reservoirs. *Nat. Gas Geosci.* **27**(8), 1367–1373 (2016)
18. Zhao, Y., Zhang, L., Shan, B.: Mathematical model of fractured horizontal well in shale gas reservoir with rectangular stimulated reservoir volume. *J. Nat. Gas Sci. Eng.* **59**(2), 67–79 (2018)
19. Yao, J., Sun, H., Fan, D., et al.: Transport mechanisms and numerical simulation of shale gas reservoirs. *J. China Univ. Petrol.* **37**(1), 91–98 (2013)
20. Guo, X., Zhou, C.: Seepage numerical model for fractured horizontal well in shale gas reservoir. *J. Southwest Petrol. Univ. (Sci. Technol. Ed.)* **36**(5), 91–96 (2014)
21. Song, H., Yu, M., Zhu, W., et al.: Numerical investigation of gas flow rate in shale gas reservoirs with nanoporous media. *Int. J. Heat Mass Transfer* **80**(20), 626–635 (2015)
22. Cai, J., Lin, D., Singh, H., et al.: Shale gas transport model in 3D fractal porous media with variable pore sizes. *Marine Petrol. Geol.* **98**, 437–447 (2018)